

Solving Reach-Avoid-Stay Problems Using Deep Deterministic Policy Gradients

Gabriel Chenevert, Jingqi Li, Achyuta Kannan, Sangjae Bae, and Donggun Lee

Abstract—Reach-Avoid-Stay (RAS) optimal control enables systems such as robots and air taxis to reach their targets, avoid obstacles, and stay near the target. However, current methods for RAS often struggle with handling complex, dynamic environments and scaling to high-dimensional systems. While reinforcement learning (RL)-based reachability analysis addresses these challenges, it has yet to tackle the RAS problem. In this paper, we propose a two-step deep deterministic policy gradient (DDPG) method to extend RL-based reachability method to solve RAS problems. First, we train a function that characterizes the maximal robust control invariant set within the target set, where the system can safely stay, along with its corresponding policy. Second, we train a function that defines the set of states capable of safely reaching the robust control invariant set, along with its corresponding policy. We prove that this method results in the maximal robust RAS set in the absence of training errors and demonstrate that it enables RAS in complex environments, scales to high-dimensional systems, and achieves higher success rates for the RAS task compared to previous methods, validated through one simulation and two high-dimensional experiments.

I. INTRODUCTION

Modern robotics and controls problems have benefited greatly from the implementation of reachability based optimal control. This refers to the control methodologies that analyze which points in a given state space can reach a target and which points are destined to collide with an obstacle. Reachability analysis has been applied to diverse and complex systems including aircraft collision avoidance [1], mobile manipulation robots [2], and unmanned aerial highway systems [3]. Both of the aforementioned are examples of reach avoid (RA) problems, where a system is driven from a starting point to a target without colliding into any obstacles. Work in RA includes leveraging reinforcement learning for efficient RA computation [4]–[10], and tackling stochastic environments [11]. Previous work [12] proposes a method which offers both computational efficiency through the use of reinforcement learning and deterministic safety guarantees via post-learning certification.

However in some scenarios, RA is insufficient as it does not consider what happens to the system after it reaches the target. For example, a camera drone must track the subject it is filming while avoiding obstacles, which requires the drone to safely maintain itself within a neighboring set of the subject. Another example is the growing push

Gabriel Chenevert, and Donggun Lee are with the Department of Mechanical and Aerospace Engineering, North Carolina State University, Raleigh, USA. {gchenev, donggun.lee}@ncsu.edu. Jingqi Li is with the Department of Electrical Engineering and Computer Sciences, University of California, Berkeley, USA. jingqili@berkeley.edu. Achyuta Kannan is with the Department of Computer Science, North Carolina State University, Raleigh, USA. ackannan@ncsu.edu. Sangjae Bae is with Honda Research Institute, sbae@honda-ri.com

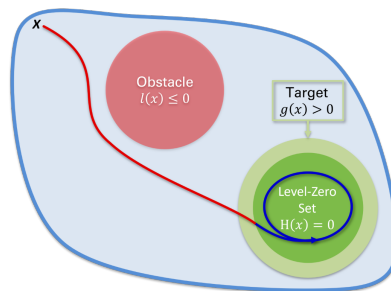


Fig. 1. The reach-avoid-stay problem can be described as controlling a system from an initial state around all obstacles to a target set where it remains. The reach-avoid-stay set (blue region) is a set of states where it is possible for our two step process to achieve the reach-avoid-stay task. First, we apply a reach-avoid policy π_V to move the system with initial state represented by the black X to the control-invariant set (green) within the target set (light green). Second, we use the invariant policy π_H to keep the system within the target set indefinitely. Note that g and l functions characterize the target set and the obstacle, respectively.

towards vertical take-off and landing (VTOL) air taxis. These aircraft must avoid obstacles while reaching a point above the landing pad and stay there before landing. A RA algorithm may waste time traversing in and out of the target.

Significant efforts have been made to develop algorithms capable of achieving reach-avoid-stay (RAS) tasks, but each method faces distinct challenges. For instance, Control-Lyapunov-Barrier based methods [13] can achieve RAS even despite disturbances, but they require the design of Control-Lyapunov-Barrier functions (CLBF), a highly challenging task for high-dimensional or complex systems due to the absence of a general design method. This problem also arises in the design of control Barrier functions [14], which ensure the state can stay within a set forever.

Some approaches attempt to address this by leveraging reinforcement learning [5], [15], but these frameworks provide a conservative subset of the RAS set and fail to identify all states that can successfully complete the RAS task, even when theoretically possible. Funnel-based control approaches [16], [17] are computationally efficient and free from the design complexities of CLBFs, however, they assume the system can stop at any point, which may not hold for dynamic vehicle applications. Existing RAS methods are unable to identify the maximum RAS set and depend on assumptions that are not generic, such as chasing a moving vehicle or a drone navigating around other drones.

To address these challenges of complex environment and scalability to high-dimensional systems, we propose a deep deterministic policy gradient (DDPG), a reinforcement learning (RL) method, for RAS problems. Building on a DDPG-based RA framework [18] that enhances scalability and

adapts to dynamic environments, we integrate robust viability kernel analysis to further enable the system to ‘stay’ within a target set. Our method consists of two steps. First, we identify a control-invariant set within the target set, ensuring the system remains inside it. Second, we perform RA analysis relative to this control-invariant set. This results in a maximal robust RAS set, as the second analysis guarantees that the system can safely reach the control-invariant set within the target, while the first control-invariance analysis ensures the system stays within the target set.

Our primary contribution to the literature is a reinforcement learning framework that provides a maximal robust RAS set, a superset of the RAS set generated by the CLBF-based method [13]. We prove that our RAS policy enables staying, in addition to RA, while the RA policy from the baseline [19] does not achieve staying. The proposed framework was thoroughly evaluated to prove that it can effectively handle complex geometries of both moving and static obstacles. We support these contributions by comparing our approach with baselines [19] in a 2D simulation and two high-dimensional experiments, vehicle chasing and VTOL scenarios, evaluating how conservative and successful our method is. Finally, we provide code samples for both training the environments demonstrated here and developing custom environments [20].

In this paper we will first define the RAS problem in Section II. Second, outline our two step approach in Section III, and third, apply this approach to two physical system demonstrations in Section IV. Finally, Section V presents the conclusion of the paper.

II. PROBLEM DEFINITION: REACH-AVOID-STAY

We consider nonlinear dynamic systems, described by

$$\mathbf{x}_{t+1} = f(\mathbf{x}_t, \mathbf{u}_t, \mathbf{d}_t), \quad (1)$$

where $\mathbf{x}_t \in \mathbb{R}^n$ is the state, $\mathbf{u}_t \in U \subset \mathbb{R}^{m_u}$ is a control, and $\mathbf{d}_t \in D \subset \mathbb{R}^{m_d}$ is a disturbance at time t . For robust analysis we consider an adversarial disturbance in the examples below. An adversarial disturbance is a disturbance that is trained or optimized at the same time as the control. For example, if the control was attempting to perform RAS tasks, the adversarial disturbance would choose some optimal disturbance each time a control was select to run the system into an obstacle or out of the target. We develop our control algorithms against an adversarial disturbance for two primary reasons:

- 1) **Robust Disturbance:** An adversarial disturbance will always provide the maximum challenge it is allowed to against a system. However, real disturbances such as wind or mobile obstacles typically lack either the ability or desire to interfere with the system intentionally. If the control is able to overcome a disturbance which has intent, it stands a good chance against unintentional disturbances.
- 2) **Unknown Error:** Every training or optimization method will inevitably make some assumptions regarding the dynamics and performance of a system. Adding a

disturbance causes the control to become slightly more conservative and can provide some buffer against these inaccuracies.

Consider an open set $T \in \mathbb{R}$ which represents the target set. We define a Lipschitz continuous bounded reward function $g(x)$ which indicates if a given state x is inside the target:

$$g(x) > 0 \Leftrightarrow x \in T \quad (2)$$

This target set is shown in light green in Fig. 1. Similarly, we consider an open set $C \in \mathbb{R}$ representing the constraint set C , a set that we want to avoid. An additional Lipschitz continuous bounded reward function $l(x)$ exists such that:

$$l(x) \leq 0 \Leftrightarrow x \in C \quad (3)$$

The constraint set is represented by the red circle labeled obstacle in Fig. 1. The precise construction of $l(x)$ and $g(x)$ is not important, although distance from the centroid of the obstacle or target is often used. Note that this paper presents a reward based framework, not a cost based framework.¹ Using these equations, we define the RAS problem as:

Problem Definition: Specify a set of states for which there exists a control policy $\pi_u : \mathbb{R}^n \rightarrow U$ that robustly achieve the RAS task: for all disturbance policies: $\pi_d : \mathbb{R}^n \rightarrow D$, the system remains in safe regions and also stays in the target set after reaching, and to find the corresponding control policy. Mathematically, the RAS set is defined as

$$\mathcal{RAS} := \left\{ x \mid \begin{array}{l} 1) \exists \pi_u \text{ s.t. } \forall \pi_d, 1) l(\mathbf{x}_t) > 0, t = 0, \dots, \text{ and} \\ 2) \exists \tau \in \{0, \dots\} \text{ s.t. } g(\mathbf{x}_t) > 0, t = \tau, \dots, \end{array} \right\}, \quad (4)$$

where \mathbf{x}_t is governed by a RAS policy π_u and a disturbance policy π_d :

$$\mathbf{x}_{t+1} = f(\mathbf{x}_t, \pi_u(\mathbf{x}_t), \pi_d(\mathbf{x}_t)), \text{ and } \mathbf{x}_0 = x. \quad (5)$$

The first condition in (4) encodes the safety condition, while the second one encodes the reach and stay conditions.

III. TWO-STEP DEEP DETERMINISTIC POLICY GRADIENTS FOR RAS

In this section, we propose a two-step RL method to find the robustly maximal RAS set and the corresponding policy under adversarial disturbances. Our approach integrates the RL frameworks for RA tasks [19] and the robust viability kernel (also known as the maximal control invariant set) [21]. In the first step, we identify the maximal control invariant set within the target set. In the second step, we apply the RA formulation, where the target is the maximal control invariant set specified in the first step. The policy derived from the RA formulation enables the system to reach the maximal control invariant set within the target set while avoiding obstacles. Once inside, the policy from the maximal control invariant set ensures that the system stays within the target. This RAS policy is a switching strategy between

¹I.E. positive numbers and rewards are considered good, and negative numbers are considered bad.

the policies derived from the maximal control invariance analysis and the RA analysis. We prove that our formulation specifies the largest possible RAS set. This implies that for any state outside our RAS set, no policy can ensure RAS under adversarial disturbances. Section III-A presents the robust viability kernel analysis. Building on this result, in Section III-B, we propose our main framework: the RAS formulation, along with its proof and algorithms.

A. Maximal Robust Control Invariant Set within the Target Set

In this subsection, we leverage the discounted formulation [19] to find the largest robust control-invariant set within the target set while avoiding obstacles. This set is referred to as the robust viability kernel:

$$\mathcal{AS} := \left\{ x \mid \exists \pi_u \text{ s.t. } \forall \pi_d, l(x_t) \text{ and } g(x_t) > 0, t = 0, \dots \right\}. \quad (6)$$

We use \mathcal{AS} to represent the robust viability kernel since it encodes the concepts of avoidance and staying.

We define a discounted-value function, $H(x)$, shown in green in Fig. 1, that characterizes the largest robust viability kernel within the target set while avoiding obstacles:

$$H(x) := \sup_{\pi_u} \inf_{\pi_d} \inf_{t=0, \dots} \gamma^t \bar{g}(x_t), \quad (7)$$

where \bar{g} characterizes the target set excluding the avoid region:

$$\bar{g}(x) := \min(g(x), l(x)). \quad (8)$$

The value of $\bar{g}(x)$ is positive if and only if the state x is in the target set and outside of the obstacle.

The following theorem presents the corresponding Bellman equations for H that characterize the robust viability kernel \mathcal{AS} and the corresponding policy that enables the system to stay in the target while avoiding obstacles.

Remark 1 *The discounted-value function H , defined in (7), is a unique solution to the following Bellman equation [22]:*

$$H(x) = \min \left\{ \bar{g}(x), \gamma \max_{u \in U} \min_{d \in D} H(f(x, u, d)) \right\}, \quad (9)$$

and the largest robust control invariant set within the target set while avoiding unsafe regions is the level-zero set of H :

$$\mathcal{AS} = \{x \mid H(x) = 0\}. \quad (10)$$

Note that $H(x)$ is non-positive for all $x \in \mathbb{R}^n$: $H(x) = 0$ for $x \in \mathcal{AS}$ and $H(x) < 0$ for $x \notin \mathcal{AS}$. Also, for $x \in \mathcal{AS}$, any control that satisfies the following equation enables staying in the target set and avoiding the obstacle for any disturbances:

$$\pi_H \in \arg \max_{u \in U} \min_{d \in D} H(f(x, u, d)), \quad (11)$$

where $\pi_H : \mathbb{R}^n \rightarrow U$ is a policy that can maintain a state within the set \mathcal{AS} .

In the following section, we will consider \mathcal{AS} as the target set in the RA formulation [19] to obtain the maximal RAS set. In this process, we need to use a value function whose super-zero-level set is \mathcal{AS} ; however, H (7) is not a suitable candidate since it is zero in \mathcal{AS} . If we use H as a function for the target set \mathcal{AS} in the RA setup, the system has no incentive to reach the target \mathcal{AS} earlier, as its value remains constant within the target. To address this issue, we design a new value function $H_g : \mathbb{R}^n \rightarrow \mathbb{R}$ in (12), whose super-zero-level set represents the same robust viability kernel \mathcal{AS} , while the values inside the set are strictly positive.

$$H_g(x) := \begin{cases} H(x) \text{ in (7),} & \text{if } H(x) < 0, \\ g(x) \text{ in (2),} & \text{otherwise.} \end{cases} \quad (12)$$

Notably, $H_g(x)$ is strictly positive for the state in the interior of \mathcal{AS} since the target set T is a subset of \mathcal{AS} and $g(x)$ is strictly positive in the interior of T , as described in (2).

B. Maximal RAS Set

In this subsection, we utilize the RA formulation from [12] to specify the RAS set and its corresponding policy, as the RAS set is the RA set where the target is the robust viability kernel within the RAS task's target set, \mathcal{AS} . We also prove that this RAS set is maximal, meaning that no state outside the RAS set can achieve the RAS task. However, the policy from the RA analysis may not fully accomplish the RAS task, as it only focuses on reaching the target while avoiding obstacles, without ensuring the system stays in the target. For the staying component, the control policy π_H from the robust viability kernel analysis guarantees that the system remains within the robust viability kernel after reaching it. To characterize the RAS set, we define another discounted-value function $V(x)$:

$$V(x) := \sup_{\pi_u} \inf_{\pi_d} \sup_{t=0, \dots} \min \{ \gamma^t H_g(x_t), \inf_{s=0, \dots, t} \gamma^s l(x_s) \} \quad (13)$$

Subsequently, the Bellman equation for V and a policy can be derived as described by the following remark.

Remark 2 *The value function V , defined in (13), is a unique solution to the following Bellman equation [19]:*

$$V(x) = \min \{ l(x), \max \{ H_g(x), \gamma \max_{u \in U} \min_{d \in D} V(f(x, u, d)) \} \}. \quad (14)$$

Also, any policy that satisfies the following equation enables reaching the robust viability kernel within the target set \mathcal{AS} while avoiding the obstacle set:

$$\pi_V(x) \in \arg \max_{u \in U} \min_{d \in D} V(f(x, u, d)), \quad (15)$$

where $\pi_V : \mathbb{R}^n \rightarrow U$ is the corresponding RA policy [19].

Now, we present our main theorem, which states that the value function V characterizes the maximal RAS set \mathcal{RAS} (4).

Theorem 1 *The super zero-level set of V (13) is the maximal robust RAS set, \mathcal{RAS} (4).*

$$\mathcal{RAS} = \{x \mid V(x) > 0\}. \quad (16)$$

Thus, $V(x) \leq 0$ if and only if $x \notin \mathcal{RAS}$.

Proof: (i) Suppose $x \in \mathcal{RAS}$. Then, there exists π_u^* such that, for all π_d , $l(x_t^*) > 0$, $t = 0, \dots$, and there exists τ^* such that $g(x_t^*) > 0$, $t = \tau, \dots$, where x^* solves (5) for π_u^*, π_d . Note that τ^* and x^* depend on π_d . These conditions can be rewritten as following: for all π_d , there exists τ^* such that $l(x_t^*) > 0$ for $t = 0, \dots, \tau^*$ and $l(x_t^*), g(x_t^*) > 0$ for $t = \tau^*, \dots$, which implies that $x_{\tau^*}^* \in \mathcal{AS}$. By (12), $H_g(x_{\tau^*}^*) = g(x_{\tau^*}^*) > 0$. Therefore, we have

$$\inf_{\pi_d} \sup_{\tau=0, \dots} \min\{\gamma^\tau H_g(x_{\tau^*}^*), \min_{t=0, \dots, \tau} \gamma^t l(x_t^*)\} > 0. \quad (17)$$

Since π_u^* may not be a maximizer for V ,

$$V(x) \geq \inf_{\pi_d} \sup_{\tau=0, \dots} \min\{\gamma^\tau H_g(x_{\tau^*}^*), \inf_{s=0, \dots, \tau} \gamma^s l(x_s^*)\} > 0. \quad (18)$$

(ii) Suppose $V(x) > 0$. Then, there exists π_V such that, for any π_d , there exists τ^* such that

$$H_g(x_{\tau^*}^*) > 0, l(x_t^*) > 0, t = 0, \dots, \tau^*, \quad (19)$$

where x^* solves (5) for π_V, π_d . Since $H_g(x_{\tau^*}^*)$ is positive, there exists another policy π_H such that, for any π_d ,

$$g(x_t^{H*}) > 0, l(x_t^{H*}) > 0, t = \tau^*, \dots, \quad (20)$$

where x_t^{H*} solves (5) for π_H, π_d , and $x_{\tau^*}^{H*} = x_{\tau^*}$.

Consider a switching policy

$$\pi_{\mathcal{RAS}}(x) = \begin{cases} \pi_V(x) & \text{if } H_g(x) \leq 0 \\ \pi_H(x) & \text{otherwise.} \end{cases} \quad (21)$$

Then, for each π_d , the corresponding state trajectory \bar{x} solving (5) for $\pi_{\mathcal{RAS}}, \pi_d$ is

$$\bar{x}_t = \begin{cases} x_t^* & t = 0, \dots, \tau^* \\ x_t^{H*} & t = \tau^*, \dots \end{cases} \quad (22)$$

Therefore, $\pi_{\mathcal{RAS}}$ satisfies, for any π_d , $l(\bar{x}_t) = l(x_t) > 0$ for $t \leq \tau^*$ by (19), $l(\bar{x}_t) = l(x_t^{H*}) > 0$ for $t > \tau^*$ by (20), and $g(\bar{x}_t) = g(x_t^{H*}) > 0$ for $t \geq \tau^*$ by (20). Thus, $x \in \mathcal{RAS}$. ■

The proof of Theorem 1 implies that if the state is within the RAS set, the system can safely reach the target using π_V and then remain in the target indefinitely using π_H .

Corollary 1 *The following policy can safely reach the target set and stay there against the worst-case disturbance if $V(x) > 0$:*

$$\pi_{\mathcal{RAS}}(x) = \begin{cases} \pi_V(x), & \text{if } H_g(x) \leq 0, \\ \pi_H(x), & \text{otherwise.} \end{cases} \quad (23)$$

In order to perform RAS task, first π_V safely maneuvers the system to the robust viability kernel within the target set.

Second, π_H enables the system to stay in the target set T indefinitely. This can be seen in Fig. 1 as the transition from red π_V control to blue π_H control once the system enters the invariant set within target set (i.e., the super zero-level set of $H_g(x)$).

C. Training Algorithm

As previously stated this methodology is algorithm agnostic. The toy example was trained using tabular Q-learning [23] to reduce the reliance on hyperparameters while evaluating the feasibility of our algorithm. Subsequent versions were constructed using deep deterministic policy gradients (DDPG) [18], [24], [25] We used Tianshou [26], a reinforcement learning library to train neural networks. We modified the DDPG policy files with the $H(x)$ and $V(x)$ Bellman equations and added zero sum game capability. When training a new set of neural nets, first we trained the $H(x)$ policy. Second, we loaded the $H(x)$ neural network in to a function which returned the value from the $H(x)$ critic when $H(x) \leq 0$ and $g(x)$ when $H(x) > 0$. This was then used as the $H_g(x)$ to train a neural network for $V(x)$. All of the resulting files, along with utility and evaluation code is available [20]. The full workflow is outlined in Algorithm 1.

IV. SIMULATION AND EXPERIMENT

In this section, we apply our method to learning RAS value functions and the associated policies. We first test our method in a two-dimensional double integrator example, where we discretize the state and action space and learn our value function via tabular Q-learning [27]. We found that the RAS set computed by our method is a superset of the invariant set obtained from the control Lyapunov barrier function. Moreover, we apply Algorithm 1 to an 18-dimensional VTOL taxi problem and a 10-dimensional drone-ground vehicle tracking problem. We observe that our learned RAS policy has a higher success rate for ensuring that the trajectory safely reaches the target set and stays than the baseline RA policy using the same target and constraint set.

A. Two Dimensional Example: Double Integrator

In this subsection, we consider a two-dimensional cart system. For this system, we utilize tabular Q-learning to train H and V , instead of DDPG's deep neural network representations, to isolate the effects of training errors. This subsection will show that our framework provides the maximal robust RAS set when compared with another RAS set computed by a baseline CLBF method [28].

Consider a two-dimensional cart system:

$$x = \begin{bmatrix} x(1) \\ x(2) \end{bmatrix} := \begin{bmatrix} x_c \\ \dot{x}_c \end{bmatrix}, \quad (26)$$

where $x(1)$ is the longitudinal position (m) of the cart along a track, and $x(2)$ is the velocity of the cart. Given its dynamics in the continuous time, we use the backward

Algorithm 1: Two-Step DDPG for RAS Problems

- 1 Training a neural network H function, H_ϕ , a neural network control policy $\pi_{H_\theta^u}$, and a neural network disturbance policy $\pi_{H_\theta^d}$ using DDPG [18], with the following modified loss functions:
 - 2 **for** training iteration for H and π_H **do**
 - 3 Update critic $H_\phi(x)$ by minimizing the loss

$$\frac{1}{S} \sum_{k=1}^S \left\| -H_\phi(x^k) + \min \left\{ \bar{g}(x^k), \gamma_{H_\phi}(f(x^k, u^k, d^k)) \right\} \right\|_2^2,$$
 where $u^k = \pi_{H_\theta^u}(x^k)$, $d^k = \pi_{H_\theta^d}(x^k)$, and S is the number of samples.
 - 4 Update actor $\pi_{H_\theta^u}$ by maximizing neural network value function H_ϕ

$$\frac{1}{S} \sum_{k=1}^S H_\phi \left(f \left(x^k, \pi_{H_\theta^u}(x^k), \pi_{H_\theta^d}(x^k) \right) \right). \quad (24)$$
 - 5 Update actor for the adversarial disturbance $\pi_{H_\theta^d}$ by minimizing the above loss (24)
 - 6 **end**
 - 7 Update $H_g(x) = \begin{cases} H_\phi(x), & \text{if } H_\phi(x) < 0, \\ g(x), & \text{otherwise} \end{cases}$ as in (12)
 - 8 Training a neural network V function, V_φ , a neural network control policy for $\pi_{V_\theta^u}$, and a neural network disturbance policy $\pi_{V_\theta^d}$ using DDPG [18], with the following modified loss functions:
 - 9 **for** training iteration for V and π_V **do**
 - 10 Update critic $V_\varphi(x)$ by minimizing the loss

$$\frac{1}{S} \sum_{k=1}^S \left\| -V_\varphi(x^k) + \min \left\{ l(x^k), \max \left\{ H_g(x^k), \gamma_{V_\varphi}(f(x^k, u^k, d^k)) \right\} \right\} \right\|_2^2,$$
 where $u^k = \pi_{V_\theta^u}(x^k)$, $d^k = \pi_{V_\theta^d}(x^k)$, and S is the number of samples.
 - 11 Update actor $\pi_{V_\theta^d}$ by maximizing control actor loss:

$$\frac{1}{S} \sum_{k=1}^S V_\varphi \left(f \left(x^k, \pi_{V_\theta^u}(x^k), \pi_{V_\theta^d}(x^k) \right) \right). \quad (25)$$
 - 12 Update actor for the adversarial disturbance $\pi_{V_\theta^d}$ by minimizing the above loss.
 - 13 **end**
-

Euler method to get the following dynamic equation in the discrete-time setting:

$$x_{t+1}(1) = x_t(1) + \Delta t x_t(2) + \Delta t^2 (u_t + d_t), \quad (27)$$

$$x_{t+1}(2) = x_t(2) + \Delta t (u_t + d_t), \quad (28)$$

where $x_t = [x_t(1); x_t(2)]$, and control ($u_t \in [-3, 3]$) and disturbance ($d_t \in [-2, 2]$) are both based on acceleration.

A target is located at the origin of the track ($x_g = 0$), and an obstacle is located at negative three ($\hat{x} = -3$). Both the obstacle and the target have a radius of one meter.

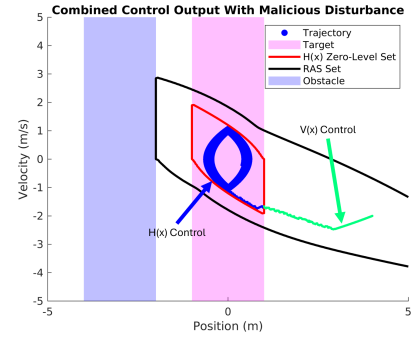


Fig. 2. This figure illustrates the maximal RAS set \mathcal{RAS} (black) and a state trajectory (green and blue) that successfully achieves the RAS task under adversarial disturbances, with an initial state of $[4.5; 0]$. π_H is applied outside the maximal viability kernel \mathcal{AS} (red) that drives the green trajectory, while π_V is applied inside it to drive the blue trajectory.

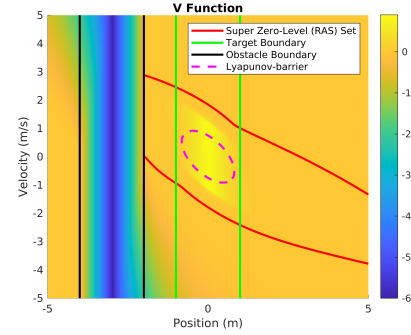


Fig. 3. This figure illustrates two RAS sets corresponding to the target set T and obstacle set C , using our framework and a baseline CLBF method [13], as well as the color map of V (13). The maximal RAS set \mathcal{RAS} (red) by our method is a superset of the RAS set provided by a baseline CLBF method (dashed magenta).

Accordingly, we design one reward function $g(x)$ and one constraint function $l(x)$ as below.

$$g(x) = 1 - |x(1) - x_g|, \quad l(x) = |x(1) - \hat{x}| - 1. \quad (29)$$

Fig. 2 illustrates the target set T , obstacle set C , the robust viability kernel \mathcal{AS} , and the maximal robust RAS set \mathcal{RAS} . We first apply tabular Q-learning to compute H , followed by constructing H_g as defined in (12). Then, we use tabular Q-learning again to compute V , with its color map shown in Fig. 3. As established by Theorem 1, any state within the maximal RAS set can successfully perform the task of reaching the target and staying within it while avoiding collisions. Fig. 2 depicts a trajectory starting from $[4; -2]$ and driven by the RAS policy $\pi_{\mathcal{RAS}}$ (23) and adversarial disturbances, where the green trajectory follows π_V , and the blue one follows π_H . The policy switching occurs at the boundary of \mathcal{AS} where the sign of H_g changes: π_V is used to safely reach \mathcal{AS} , and π_H is used to safely remain within it.

Fig. 3 shows comparison between our method and a baseline CLBF method [13]. As supported by Theorem 1, our method provides the maximal RAS set \mathcal{RAS} , which is also illustrated in this figure, demonstrating that our maximal RAS set \mathcal{RAS} is a superset of the RAS set provided by the baseline method. The volume of the maximal RAS set \mathcal{RAS} is 17.02, compared to the Lyapunov baseline at 1.98.

Method	VTOL		Chase	
	Safely Reach	and Stay	Safely Reach	and Stay
RAS policy	94.3	93.0	98.8	94.1
RA policy	98.9	0	99.8	91.4

TABLE I
SUCCESS RATES FOR THE CHASE AND VTOL ENVIRONMENTS
DEMONSTRATING RAS CAPABILITY.

B. High-Dimensional System Experiments

In this subsection, we present two high-dimensional experiments to evaluate the RAS policies and RAS sets learned by Algorithm 1. Considering a target set T and a constraint set C , we compare the learned RAS policy and RAS set with the RA policy and RA set learned using the method from [19].

1) *VTOL Taxi*: Consider an air taxi flying passengers between buildings in a city. The taxi must avoid collisions with buildings and other aircraft while moving to a drop off location. In this demonstration, there is one ego drone which fills the role of the air taxi, and two drones which act other air taxis which the ego drone must avoid. We model this system with an 18-dimensional state $x = [p^e, v^e, p^1, v^1, p^2, v^2]$, where $p^e \in \mathbb{R}^3$ and $v^e \in \mathbb{R}^3$ represent the ego drone's position and velocity, respectively. p^1 and v^1 denote the position and velocity of the first autonomous drone, and p^2 and v^2 represent those of the second autonomous drone. The ego drone uses the following dynamics.

$$p_{t+1}^e = p_t^e + \Delta t v_t^e \quad (30)$$

$$v_{t+1}^e = v_t^e + \Delta t (u_t + d_t) \quad (31)$$

where $u_t \in \mathbb{R}^3$ is a velocity input to the drone, and the disturbance $d_t \in \mathbb{R}^2$ represents wind and dynamics modeling errors. Each of the two obstacle drones is modeled with double integrator dynamics, where the control input is designed as PD control to follow a fixed target, with the acceleration bounded between -0.5 and 0.5. We use the following $l(x)$ and $g(x)$ equations:

$$l(x) = \min \left((p^e - p^1) - 2r_d, (p^e - p^2) - 2r_d, \sqrt{(p^e(1) - b(1))^2 + (p^e(2) - b(2))^2 - r_d} \right),$$

$$g(x) = r_t - \sqrt{(p^e(1) - t(1))^2 + (p^e(2) - t(2))^2 + (p^e(3) - t(3))^2},$$

where r_d is the radius of the drone, b is the position of the building, t is the position of the target, and r_t is the radius of the target.

Comparison with the baseline: Following offline training of control and disturbance policies using DDPG, one thousand initial states were randomly sampled from within the learned RAS set. We simulate trajectories from those sampled initial conditions under the trained RAS and RA control policies and randomly sampled disturbances. The results are summarized in Table I. In particular, the column ‘‘Safely reach’’ of Table I represents the ratio of initial stats that can safely reach the target set. The column ‘‘and Stay’’ indicates the percentage of the thousand initial conditions that was able

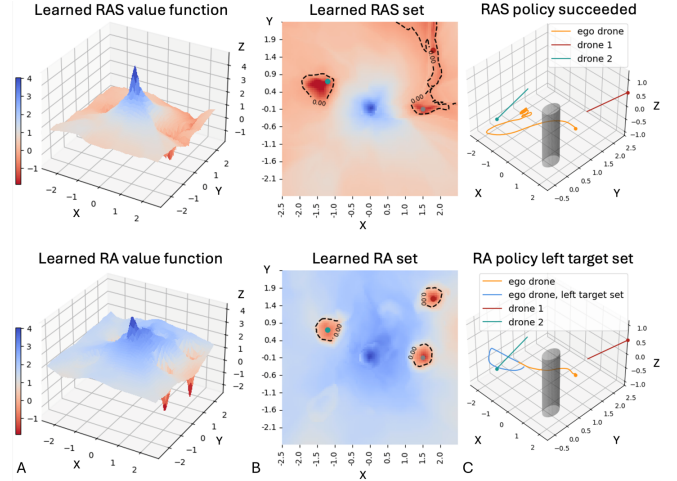


Fig. 4. Visualization of the learned RAS value function, RA value function, and the simulation of their policies for the VTOL example. We parameterize both the RA and RAS value functions and their associated policies using 4-layer ReLU neural networks, each with 512 neurons per layer. A: The learned value functions, where the x and y positions of the ego drone are varied, while the remaining 10 state dimensions are fixed. B: The learned RAS set (the super-zero level set of the RAS value function) and the learned RA set (the super-zero level set of the RA value function). In particular, the red dot represents drone 1, the green dot represents drone 2, and the grey dot represents the static cylinder obstacle. The deep red areas near these objects indicate that both value functions accurately capture the safety information around them. C: Simulation trajectories for both the RAS and RA policies. Under the RAS policy, the trajectory **safely reaches and stays within the target set**. Conversely, under the RA policy, the trajectory reaches the target set safely but with a high speed, and therefore it **leaves after entering**.

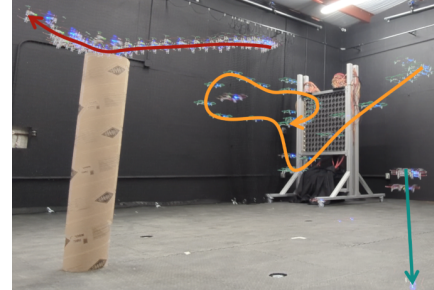


Fig. 5. VTOL Demonstration. The orange line represents the ego drone. The red and teal lines represent obstacle drones 1 and 2 respectively.

to both safely reach and then remain in the target set. The RAS policy was able to achieve a high success rate of 93.0%. From trajectories which were selected for manual review, it was noted that RA policy would reach the target, but have such a high speed upon entry that it was unable to stay and instead exited the target before looping around to reach it again. This behavior can be observed in Fig. 4C. The result was not a single RA trajectory succeeded.

The RAS and RA value functions are shown in Fig. 4A,B show how each algorithm values the state space. Note that the RAS set is smaller than the RA set, denoted by the white and blue side of the level-zero dashed lines. Additionally, the RAS set includes information about the predicted future trajectories of the obstacle drones based on where it has learned they are likely to travel to.

Validation via Experiment: Physical testing was also conducted using small drones and a cardboard model of the

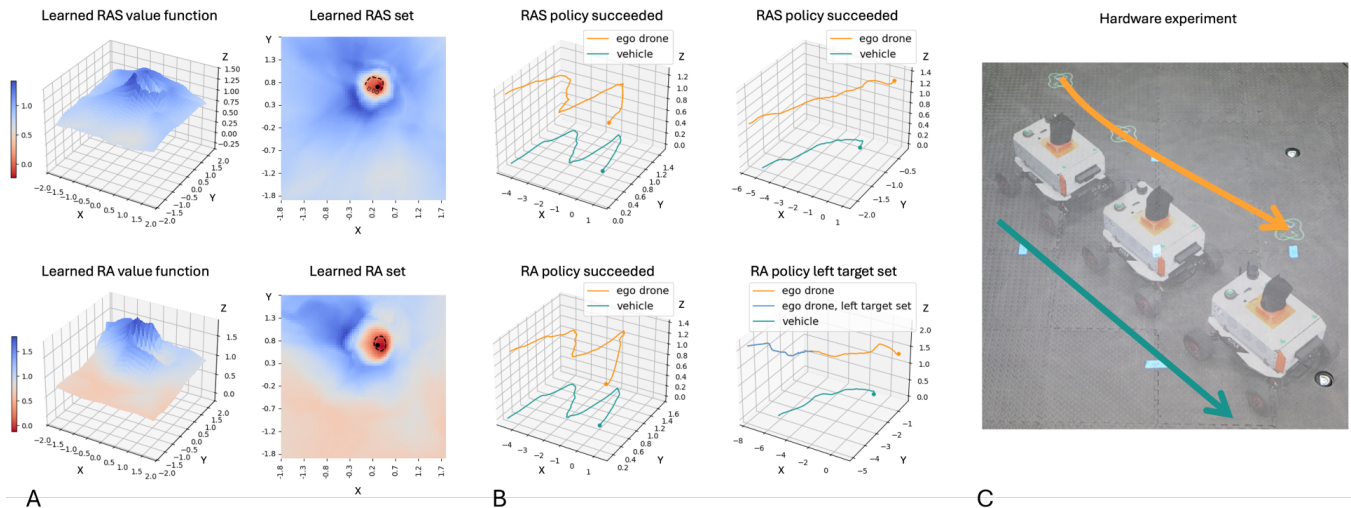


Fig. 6. Visualization of the learned RA and RAS results for drone-vehicle chasing problem. Both the RA and RAS policies, as well as their corresponding value functions, are parameterized using 4-layer ReLU neural networks. The policy networks have 512 neurons per layer, while the value function networks have 768 neurons per layer. A: RA and RAS value functions. The dashed black lines represent the level zero set surrounding the obstacle (ground vehicle) represented by a black dot. Here we visualize the learned RAS set by varying the x and y positions of the ego drone, with the z -axis position of the drone evaluated at 0.6 meters. It represents a challenging situation where the drone wants to stay in the neighboring set of the ground vehicle but also avoid violating safety constraint. B: Simulated trajectories using the RAS policy and RA policy. The orange lines represent the trajectory of the drone, and the teal lines represent the ground vehicle trajectory. We observe that while the RA policy can effectively chase the vehicle at times, it may also **leave the target set after reaching it**. C: Hardware experiment trajectory. The orange lines represent the trajectory of the drone, and the teal lines represent the ground vehicle trajectory.

building. The result from a sample test are shown in Fig. 5. The ego drone shown in green is able to avoid both red obstacle drones before orbiting in the center of the environment where the target is.

2) A drone chasing an unpredictable ground vehicle:

Consider applications such as a camera drone or a delivery drone that safely track a target and aim to stay close to it. In this scenario, we model a ground vehicle and a drone, where the ground vehicle is manually controlled, and the drone autonomously follows it, maintaining proximity while avoiding collisions.

We model the system with a 10-dimensional state vector $x = [x(1), \dots, x(10)] := [p^d, v^d, p^v, v^v]$, where $p^d \in \mathbb{R}^3$ and $v^d \in \mathbb{R}^3$ denote the 3D position and velocity of the drone, respectively, and $p^v \in \mathbb{R}^2$ and $v^v \in \mathbb{R}^2$ represent the 2D position and velocity of the ground vehicle. The system evolves according to the following dynamics:

$$\begin{aligned} p_{t+1}^d &= p_t^d + \Delta t v_t^d & v_{t+1}^d &= v_t^d + \Delta t u_t \\ p_{t+1}^v &= p_t^v + \Delta t v_t^v, & v_{t+1}^v &= v_t^v + \Delta t d_t, \end{aligned} \quad (32)$$

where $u_t \in \mathbb{R}^3$ is an acceleration input to the drone, and the disturbance $d_t \in \mathbb{R}^2$ represents the 2D acceleration of the ground vehicle. The target is represented as a sphere located one meter above the vehicle. The obstacle is modeled as a sphere surrounding the ground robot. The obstacle and target are represented by:

$$\begin{aligned} l(x) &= \sqrt{(p^d(1) - p^v(1))^2 + (p^d(2) - p^v(2))^2 + (p^d(3) - o(3))^2}, \\ g(x) &= r_t - \sqrt{(p^d(1) - p^v(1))^2 + (p^d(2) - p^v(2))^2 + (p^d(3) - t(3))^2}, \end{aligned}$$

where $o(3)$ is the height of the obstacle, in this case .28 meters, $t(3)$ is the height of the target, 1 meter, and r_t is the radius of the target.

Comparison with the baseline: One thousand trajectories from inside the RAS set defined by the super-zero-level-set of the trained $V(x)$ were tested in simulation in the same manner as the VTOL demonstration. The results can be found in Table I. As before, RAS policy was able to achieve a high success rate for both safely reaching, and staying of 98.8% and 94.1% respectively. RA policy was out performed in staying once again, it did score significantly higher in the chase environment compared to the VTOL environment at 91.4% staying compared to no successful stays in the VTOL. This is likely due to the nature of the disturbance. RA policy fails to stay when it allows itself to reach a velocity high enough that it can not stop within the target. Under normal circumstances, this is acceptable to RA policy because it is not concerned with time steps after it hits the target. However, in the chase game, the target is able to move and if the drone reached a very high velocity the target could side step it and cause it to overshoot. Thus, RA policy must adopt a conservative velocity compared to the VTOL environment to prevent the target from being able to avoid it.

The learned value functions and sets shown in Fig. 6A are more similar than in the previous VTOL example. However, they do indicate that RAS policy cares less about directionality when approaching the target set. This may be due to the more cautious nature of RAS policy in general causing it to be less concerned with the current velocity of the ground vehicle as it will be able to match its trajectory regardless. Simulated trajectories presented in Fig. 6B also illustrate some of the differences between RA and RAS policies. While both are able to follow a zig-zag pattern, RA policy struggles when the ground vehicle is able to build up speed across a long trajectory and cause it to overshoot.

Validation via Experiment: We conducted the physical

demonstration using one drone running Crazyswarm2 [29] remotely and a ground vehicle which was manually controlled. The human control to the vehicle was considered by the ego drone as unpredictable disturbance. Both were tracked by an infrared camera motion tracking system which directly provided position updates. We composited video of the ground robot and drone into Fig. 6C. The ground robot drove from the top left of the image to the bottom right. The drone initially started in the center of the environment before moving to above the ground robot without hitting it. It then stayed within the target set above the ground robot as it followed the ground robot across the environment.

V. CONCLUSION

This paper presents a two-step deep deterministic policy gradient method to address the RAS problem, effectively managing complex environments and high-dimensional systems. By building on reachability formulations, we prove that our approach yields the maximal RAS set, encompassing any RAS set produced by other baselines, including CLBF methods. Simulations and real-world experiments demonstrate the advantages of our method: it not only delivers the maximal RAS set as a superset of those from the baselines but also achieves a higher success rate in the RAS task compared to traditional RA formulations. In future work, we will provide deterministic performance guarantees for the learned RAS policy by developing efficient post-learning verification methods.

REFERENCES

- [1] M. Prandini and J. Hu, "Application of reachability analysis for stochastic hybrid systems to aircraft conflict prediction," in *2008 47th IEEE Conference on Decision and Control*, pp. 4036–4041, ISSN: 0191-2216. [Online]. Available: <https://ieeexplore.ieee.org/document/4739248>
- [2] S. Jauhari, J. Peters, and G. Chalkatzaki, "Robot learning of mobile manipulation with reachability behavior priors," vol. 7, no. 3, pp. 8399–8406. [Online]. Available: <http://arxiv.org/abs/2203.04051>
- [3] M. Chen, Q. Hu, J. F. Fisac, K. Akametalu, C. Mackin, and C. J. Tomlin, "Reachability-based safety and goal satisfaction of unmanned aerial platoons on air highways," vol. 40, no. 6, pp. 1360–1373, publisher: American Institute of Aeronautics and Astronautics. [Online]. Available: <https://arc.aiaa.org/doi/10.2514/1.G000774>
- [4] R. E. Allen, A. A. Clark, J. A. Starek, and M. Pavone, "A machine learning approach for real-time reachability analysis," in *2014 IEEE/RSJ International Conference on Intelligent Robots and Systems*, pp. 2202–2208, ISSN: 2153-0866. [Online]. Available: <https://ieeexplore.ieee.org/document/6942859>
- [5] C. Dawson, Z. Qin, S. Gao, and C. Fan, "Safe nonlinear control using robust neural lyapunov-barrier functions." [Online]. Available: <http://arxiv.org/abs/2109.06697>
- [6] K.-C. Hsu, V. Rubies-Royo, C. J. Tomlin, and J. F. Fisac. Safety and liveness guarantees through reach-avoid reinforcement learning. [Online]. Available: <https://arxiv.org/abs/2112.12288v1>
- [7] K.-C. Hsu, H. Hu, and J. F. Fisac. The safety filter: A unified view of safety-critical control in autonomous systems. [Online]. Available: <https://arxiv.org/abs/2309.05837v1>
- [8] K.-C. Hsu, A. Z. Ren, D. P. Nguyen, A. Majumdar, and J. F. Fisac. Sim-to-lab-to-real: Safe reinforcement learning with shielding and generalization guarantees. [Online]. Available: <https://arxiv.org/abs/2201.08355v4>
- [9] K.-C. Hsu, D. P. Nguyen, and J. F. Fisac. ISAACS: Iterative soft adversarial actor-critic for safety. [Online]. Available: <https://arxiv.org/abs/2212.03228v3>
- [10] J. F. Fisac, N. F. Lugovoy, V. Rubies-Royo, S. Ghosh, and C. J. Tomlin, "Bridging hamilton-jacobi safety analysis and reinforcement learning," in *2019 International Conference on Robotics and Automation (ICRA)*, pp. 8550–8556, ISSN: 2577-087X. [Online]. Available: <https://ieeexplore.ieee.org/document/8794107>
- [11] S. Summers, M. Kamgarpour, J. Lygeros, and C. Tomlin, "A stochastic reach-avoid problem with random obstacles," in *Proceedings of the 14th international conference on Hybrid systems: computation and control*, ser. HSCC '11. Association for Computing Machinery, pp. 251–260. [Online]. Available: <https://dl.acm.org/doi/10.1145/1967701.1967738>
- [12] J. Li, D. Lee, S. Sojoudi, and C. J. Tomlin, "Infinite-horizon reach-avoid zero-sum games via deep reinforcement learning." [Online]. Available: <http://arxiv.org/abs/2203.10142>
- [13] Y. Meng and J. Liu, "Lyapunov-barrier characterization of robust reach-avoid-stay specifications for hybrid systems." [Online]. Available: <http://arxiv.org/abs/2211.00814>
- [14] A. D. Ames, S. Coogan, M. Egerstedt, G. Notomista, K. Sreenath, and P. Tabuada, "Control barrier functions: Theory and applications," in *2019 18th European Control Conference (ECC)*, pp. 3420–3431. [Online]. Available: <https://ieeexplore.ieee.org/document/8796030>
- [15] O. So, Z. Serlin, M. Mann, J. Gonzales, K. Rutledge, N. Roy, and C. Fan, "How to train your neural control barrier function: Learning safety filters for complex input-constrained systems," pp. 11 532–11 539, conference Name: 2024 IEEE International Conference on Robotics and Automation (ICRA) ISBN: 9798350384574 Place: Yokohama, Japan Publisher: IEEE. [Online]. Available: <https://ieeexplore.ieee.org/document/10610418/>
- [16] R. Das and P. Jagtap. Funnel-based control for reach-avoid-stay specifications. [Online]. Available: <https://arxiv.org/abs/2308.15803v1>
- [17] —, "Prescribed-time reach-avoid-stay specifications for unknown systems: A spatiotemporal tubes approach," vol. 8, pp. 946–951, conference Name: IEEE Control Systems Letters. [Online]. Available: <https://ieeexplore.ieee.org/document/10540043>
- [18] S. Li, Y. Wu, X. Cui, H. Dong, F. Fang, and S. Russell, "Robust multi-agent reinforcement learning via minimax deep deterministic policy gradient," vol. 33, no. 1, pp. 4213–4220, number: 01. [Online]. Available: <https://ojs.aaai.org/index.php/AAAI/article/view/4327>
- [19] J. Li, D. Lee, J. Lee, K. S. Dong, S. Sojoudi, and C. Tomlin, "Certifiable deep learning for reachability using a new lipschitz continuous value function." [Online]. Available: <http://arxiv.org/abs/2408.07866>
- [20] G. Chenevert, "Day-star/RASDemo." [Online]. Available: <https://github.com/Day-Star/RASDemo>
- [21] J.-P. Aubin, A. M. Bayen, and P. Saint-Pierre, "Regulation of control systems," in *Viability Theory: New Directions*, J.-P. Aubin, A. M. Bayen, and P. Saint-Pierre, Eds. Springer, pp. 437–484. [Online]. Available: https://doi.org/10.1007/978-3-642-16684-6_11
- [22] F. L. Lewis, D. L. Vrabie, and V. L. Syrmos, *Optimal control*, 3rd ed. Wiley.
- [23] C. J. C. H. Watkins and P. Dayan, "Q-learning," vol. 8, no. 3, pp. 279–292. [Online]. Available: <https://doi.org/10.1007/BF00992698>
- [24] T. P. Lillicrap, J. J. Hunt, A. Pritzel, N. Heess, T. Erez, Y. Tassa, D. Silver, and D. Wierstra, "Continuous control with deep reinforcement learning." [Online]. Available: <http://arxiv.org/abs/1509.02971>
- [25] D. Silver, G. Lever, N. Heess, T. Degris, D. Wierstra, and M. Riedmiller, "Deterministic policy gradient algorithms," in *Proceedings of the 31st International Conference on Machine Learning*. PMLR, pp. 387–395, ISSN: 1938-7228. [Online]. Available: <https://proceedings.mlr.press/v32/silver14.html>
- [26] "thu-ml/tianshou," original-date: 2018-04-16T22:47:38Z. [Online]. Available: <https://github.com/thu-ml/tianshou>
- [27] R. S. Sutton and A. Barto, *Reinforcement learning: an introduction*, second edition ed., ser. Adaptive computation and machine learning. The MIT Press.
- [28] J.-J. E. Slotine, W. Li, and others, *Applied nonlinear control*. Prentice hall Englewood Cliffs, NJ, vol. 199, number: 1.
- [29] "IMRCLab/crazyswarm2," original-date: 2021-11-04T17:12:54Z. [Online]. Available: <https://github.com/IMRCLab/crazyswarm2>